JOURNAL OF AIRCRAFT
Vol. 33, No. 3, May–June 1996

Damage Tolerance and Failure Analysis of a Composite Geodesically Stiffened Compression Panel

Marshall Rouse* and Damodar R. Ambur†
NASA Langley Research Center, Hampton, Virginia 23681-0001

A geodesically stiffened continuous-filament composite structural concept has been designed for a transport aircraft fuselage application and fabricated using an automated manufacturing process. Both large panels and element specimens derived from these panels have been experimentally and analytically investigated when subjected to axial compression to understand their buckling, postbuckling, and failure responses. The primary failure mode for this structural concept is skin-stiffener separation in the skin postbuckling load range. The large panels are subjected to low-speed impact damage and tested to failure in axial compression to evaluate the damage tolerance of this structural concept. These results suggest that damage to the stiffener and a stiffener intersection point from the skin side do not influence the failure load or failure mode of this structural concept. Nonlinear finite element analysis using a detailed element specimen model indicates that failure of this specimen may have initiated at the skin-stiffener flange region close to the stiffener intersection. When the skin is in the postbuckling range at four times its initial buckling load, the interlaminar shear stress concentrations at a region where the stiffener makes a 20-deg turn away from the stiffener intersection seem to initiate panel failure.

Introduction

STRUCTURAL efficiency is an important aspect of the design of cost-effective aircraft structures. This structural efficiency requirement is accomplished in many instances through increased use of composite structures that consist of flat or curved panels that are reinforced by stiffeners. These stiffeners are either cocured, bonded, or bolted to the panel skin. Of these attachment concepts, stiffened composite structures produced by cocuring are the most cost effective because of reduced part count. Although many manufacturing processes are available to produce cocured structures, automated tow or tape placement and filament or tape winding methods have emerged as some of the more viable ones.

Continuous-filament grid-stiffened structures are stiffened structures that are produced by winding or laying continuous filaments in an automated process. Different structural configurations such as orthogrid (stiffeners placed in mutually perpendicular directions), isogrid (stiffeners placed in an equilateral triangular pattern), or any general grid configuration (stiffeners placed in arbitrary directions), may be produced using this manufacturing process. Geodesically stiffened structures that utilize continuous-filament composite material for stiffener construction are very efficient for aircraft fuselage application since the structure is very effective in carrying loads because of bending, shear, torsion, and internal pressure. The structural efficiency combined with cost-effective methods of manufacturing make geodesically stiffened structures very attractive for commercial transport aircraft structural applications. Geodesically stiffened structures are also very damage tolerant since there are multiple paths available to redistribute the load because of the nonprismatic nature of the structure.

The continuous-filament isogrid structure was first produced in 1976 in an effort to develop efficient, low-cost structures. The compressive buckling and dynamic behaviors of this isogrid structural concept were studied in Refs. 1 and 2. The damage tolerance of this structural concept when subjected to uniaxial compression was demonstrated experimentally and validated analytically with finite element analysis results.[3,4] A design study conducted on a Lockheed C-130 transport aircraft center fuselage using continuous-filament grid-stiffened concepts such as isogrid and orthogrid concepts demonstrated a weight savings of 20–30% compared to the conventional metallic design.[5] The tailboom of Bell Helicopter Textron's advanced composite airframe program candidate has a grid-type construction reinforced by fiberglass–epoxy/polyimide–foam sandwich longerons.[6] Structural analysis and design optimization of a geodesically stiffened wing rib panel were performed in Ref. 7. Although there have been many studies and applications involving continuous-filament grid-stiffened structures as summarized earlier, there have been very few studies on the failure and damage tolerance of these structures when loaded as a panel supported along all edges. The only effort to determine the failure modes for grid-stiffened panels was reported in Ref. 8, where finite element analysis results for a composite isogrid panel were presented for different skin-stiffener interfaces determined through a global–local analysis approach. Their results were not used in conjunction with actual test panel failure modes to demonstrate the predictive capability of this analysis approach.

This article describes a geodesically stiffened panel concept that was designed for a fuselage application with a combined axial compression and shear loads of 3000 and 600 lb/in., respectively. This weight-efficient structural concept has stiffeners placed at an angle to the axial direction such that the stiffeners carry most of the axial and in-plane shear load components. This panel has been tested in uniaxial compression both without and with low-speed impact damage to study the buckling and postbuckling response of the structure. The purpose of the low-speed impact damage test is to demonstrate the damage tolerance of the structural concept with barely visible impact damage. Finite element analysis has been used to predict the undamaged panel response and the analytical buck-

Received March 13, 1994; presented at the AIAA 35th Structures, Structural Dynamics, and Materials Conference, Hilton Head, SC, April 18–20, 1994; revision received Nov. 30, 1995; accepted for publication Dec. 20, 1995. Copyright © 1996 by the American Institute of Aeronautics and Astronautics, Inc. No copyright is asserted in the United States under Title 17, U.S. Code. The U.S. Government has a royalty-free license to exercise all rights under the copyright claimed herein for Governmental purposes. All other rights are reserved by the copyright owner.

*Aerospace Engineer, Aircraft Structures Branch, Structures Division. Member AIAA.

†Senior Aerospace Engineer, Structural Mechanics Branch, Structures Division. Associate Fellow AIAA.

ling load. This article summarizes experimental results for the undamaged and damaged panels, and analytical results for the undamaged panel. This article also presents experimental and analytical results for the skin-stiffener element specimens that were derived from this stiffened panel. Detailed two-dimensional analysis results are used to examine the failure modes for structures of this type of construction. These element specimens were tested and analyzed to better understand the failure modes observed in the panel failure test. Information on the failure modes and damage tolerance for this structural concept adds significantly to the database for this category of grid-stiffened structures, as similar concepts are being considered for the keel region of advanced fuselage structures.

Specimen Description and Experimental Procedure

The specimens tested in this investigation were fabricated from commercially available Hercules, Inc., AS4 graphite fiber, preimpregnated with Hercules 3502 epoxy resin (AS4/3502). The skin of the specimens was made from five-ply laminates with a $(45/90/+45)_s$ stacking sequence. This skin had a fiber crossover pattern across the midsection of the panel to simulate a filament wound skin feature. The stiffeners were oriented at 20 to the longitudinal axis of the test panel. The stiffeners were made of unidirectional tows of Hercules, Inc., AS4/3502 graphite–epoxy material overwrapped with AS4/3502 graphite–epoxy fabric material and were secondarily bonded to the skin. Two frame clips were made of woven AS4/3502 graphite–epoxy fabric and secondarily bonded to the skin at a distance of 10 in. on either side of the horizontal centerline of the specimen. Also, a buffer strip made from unidirectional tow material was embedded in the skin across the panel width at each of the frame clip locations to simulate fail-safe straps in a fuselage. A total of three specimens was tested in this investigation. All of the specimens were 40 in. long. Two of the specimens were 14.56 in. wide, and the third was 29.12 in. wide. The ends of the specimens were potted and ground flat and parallel to ensure uniform load introduction. The unloaded sides of the specimens were supported with knife edges. A sketch of the typical test specimen including the local details is shown in Fig. 1. The axial compression testing of these panels was conducted using a 1-million-lb capacity hydraulic test machine.

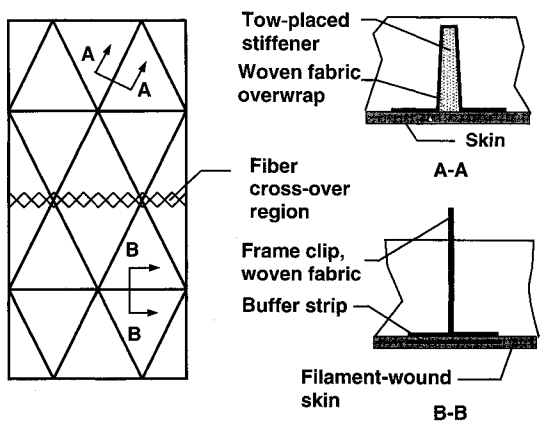

Fig. 1 Specimen details.

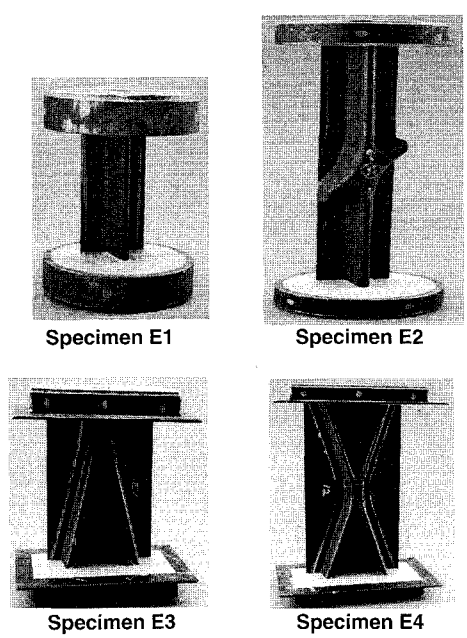

Fig. 2 Element test specimens.

Element specimens that represent four critical regions of the panel were cut from one of the large panels. Photographs of four types of element specimens are shown in Fig. 2. These element specimens were tested to failure in uniaxial compression as wide columns to determine the response mechanisms associated with the failure of the large test panels. Strain and displacement data were obtained for all of the panel tests and element tests. Strain data were obtained using 350-Ω resistance wire strain gauges with a 0.187-in. gauge length. Displacement data were recorded using direct current displacement transducers. In addition, qualitative descriptions of the specimen out-of-plane deflections at different load levels were obtained using shadow moiré interferometry.

Results and Discussion

Experimental Results

In this section of this article, compression test results for the undamaged panels and element specimens will be presented first. Results from compression-loaded, air gun, impact-damaged panels will be presented and discussed.

Undamaged Compression Panels

A summary of specimen end-shortening results for all of the panels that were tested in compression without impact damage is shown in Fig. 3. Applied load P normalized by the width of the test section b, plotted as a function of end-shortening U, normalized by the length of the test section L, is shown on the left of the figure. Results for the 29.12- and 14.56-in.-wide panels are represented by the circle and square symbols, respectively. The theoretical buckling loads obtained from the finite element analysis are indicated by the open symbols. The experimental failure loads of the panels are indicated by the filled symbols. The panels buckled at a normalized applied load of approximately 1400 lb/in. All of the panels tested without damage failed at a value of applied load greater than the theoretical buckling load. The normalized failure loads for the 29.12- and 14.56-in.-wide panels are 3312 and 3540 lb/in., respectively.

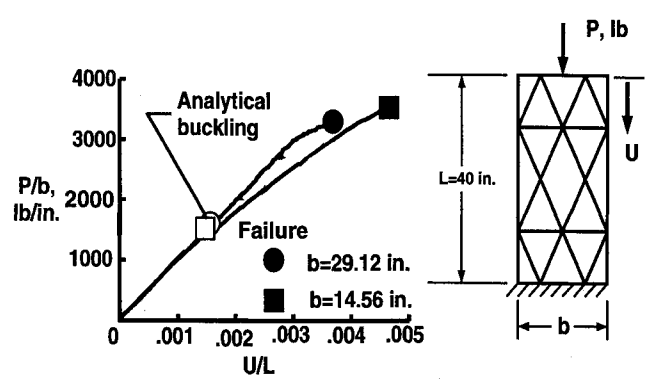

Fig. 3 Summary of end-shortening results for specimens tested without impact damage.

Out-of-plane deflection W measured at the intersection of a frame and stiffeners located on the vertical midsection of the panel, normalized by the skin thickness t, is shown in Fig. 4 as a function of the normalized load. Failure of the panels is indicated by the filled circle. All of the panels deformed out-of-plane prior to buckling when loaded. The 29.12-in.-wide specimen exhibited the most out-of-plane deflection during loading with a maximum value of over six times the skin thickness. The 14.56-in.-wide panel had a maximum out-of-plane deflection of approximately four times the skin thickness. The difference in out-of-plane response and failure load between the two panels is predominately a specimen width effect.

A comparison of typical surface strain results for a 14.56-in.-wide panel tested without impact damage is presented in Fig. 5 as a function of normalized load. The surface strain ε_x results were recorded from back-to-back strain gauges oriented parallel to the direction of applied loading at two locations on the skin. Surface strain results from back-to-back strain gauges at location A, which is at the center of the specimen on the skin, are indicated by the filled circles. Surface strain results from back-to-back strain gauges at location B, which is away from the center of the specimen on the skin, are indicated by the filled square. The panel had a maximum compressive strain of approximately 0.008 in./in., and a maximum tensile value of approximately 0.002 in./in. at the center of the specimen at failure. The divergence of the back-to-back strain gauge results at the center of the panel suggests that bending strain at the center of the specimen is because of local buckling of the skin as the panel was loaded to failure. The discontinuities in the surface strain results measured at the center of the panel suggest that a redistribution of load occurred at approximate values for normalized load of 1500 and 2500 lb/in. The redistribution of load was because of a combination of changes in the skin local buckling mode and local failures at the skin-stiffener interface and fiber crossover region. The panel had a maximum compressive strain of approximately 0.001 in./in. at location

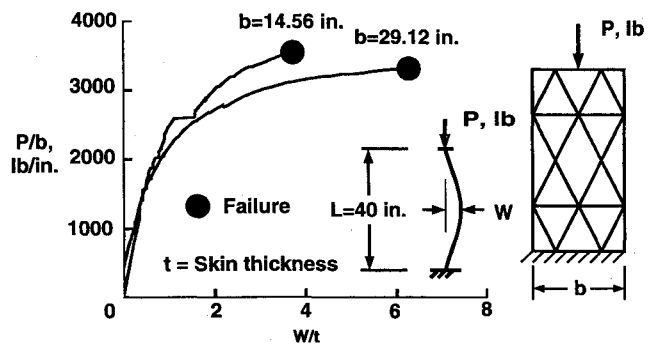

Fig. 4 Summary of out-of-plane displacement results for specimens tested without impact damage.

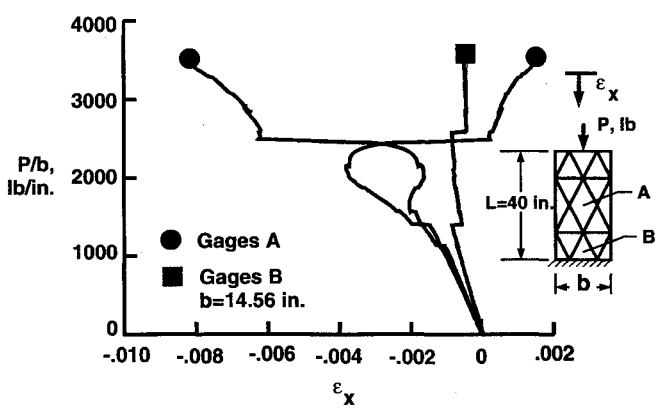

Fig. 5 Typical surface strain results for a 14.56-in.-wide panel.

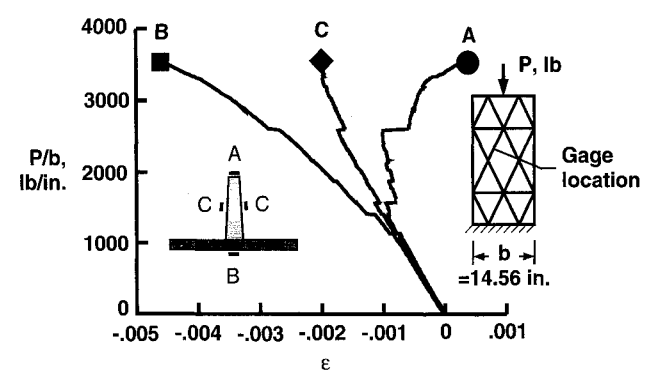

Fig. 6 Typical stiffener axial strain results for a 14.56-in.-wide panel.

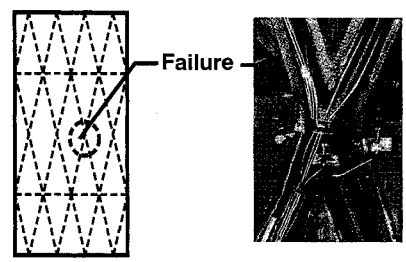

Fig. 7 Failure characteristics of geodesically stiffened compression panel.

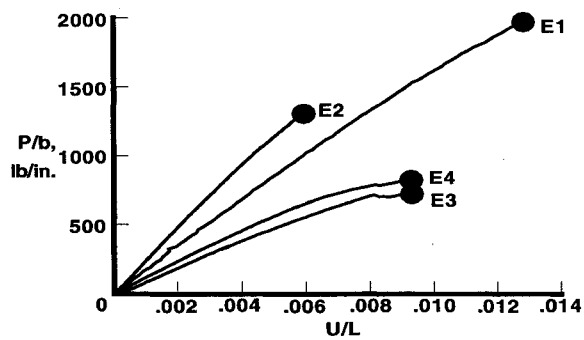

Fig. 8 Summary of experimental end-shortening results for element specimens.

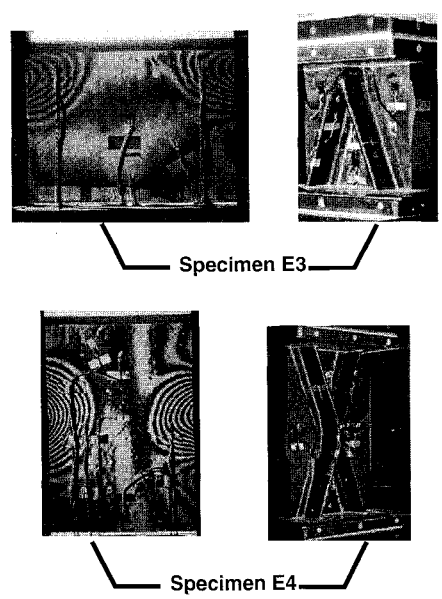

Fig. 9 Out-of-plane displacement profiles and failure modes for element specimens E3 and E4.

B. The discontinuities in the load–strain curve for surface strain results measured at location B suggest that local failures caused redistributions of the load in the panel as it was loaded to failure.

Typical stiffener axial strain results for a 14.56-in.-wide panel tested without impact damage is presented in Fig. 6 as a function of the normalized applied load. The axial strain ε results were recorded from strain gauges oriented parallel to the direction of the stiffener at locations midway between stiffener intersections. Axial strain data at location A on the crown of the stiffener are indicated by the filled circle. Surface strain data on the skin below the stiffener are indicated by the filled square. Axial strain data at locations C on the sides of the stiffener are indicated by the filled diamond. A maximum tensile strain at failure of approximately 0.005 in./in. was measured at location A. The panel had a maximum compressive strain at location B of approximately 0.0047 in./in. at failure. Divergence of the axial strain data at locations A and B suggests that bending strains occurred about a plane parallel to the midplane of the skin as the panel was loaded into the postbuckling range. The panel had a maximum compressive strain value at locations C of approximately 0.002 in./in. at failure. The results at locations C also suggest that no lateral bending of the stiffener occurred. Also, the discontinuities in the load-strain curves shown in Fig. 6 suggest that a redistribution of load occurred in the panel because of local failures prior to the failure of the panel.

Typical failure characteristics of the geodesically stiffened compression panel tested without impact damage are shown in Fig. 7. The sketch on the left of the figure shows the skin side of the failed panel. The panel failed because of separation of the skin from the stiffeners across the middle of the panel in addition to the failure along the fiber crossover region. The photograph on the right of the figure shows a close-up of one of the local failure modes of the panel.

Undamaged Element Specimens

The primary failure mode for the damaged grid-stiffened structure was separation of the skin from the stiffener at the midsection of the panel in addition to failure along the fiber crossover region. A secondary failure mode was a scissoring action in the overwrap at the stiffener intersection region. To further investigate these failure modes, four types of specimens, shown in Fig. 2, have been tested in axial compression.

Typical end-shortening results for the four types of element specimens are shown in Fig. 8. Specimen E3 is essentially a

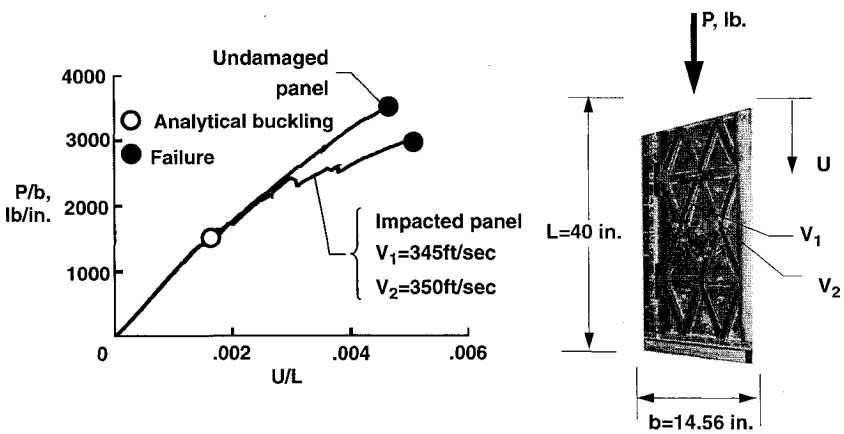

Fig. 10 Summary of end-shortening results for specimens with low-speed impact damage at two stiffener locations.

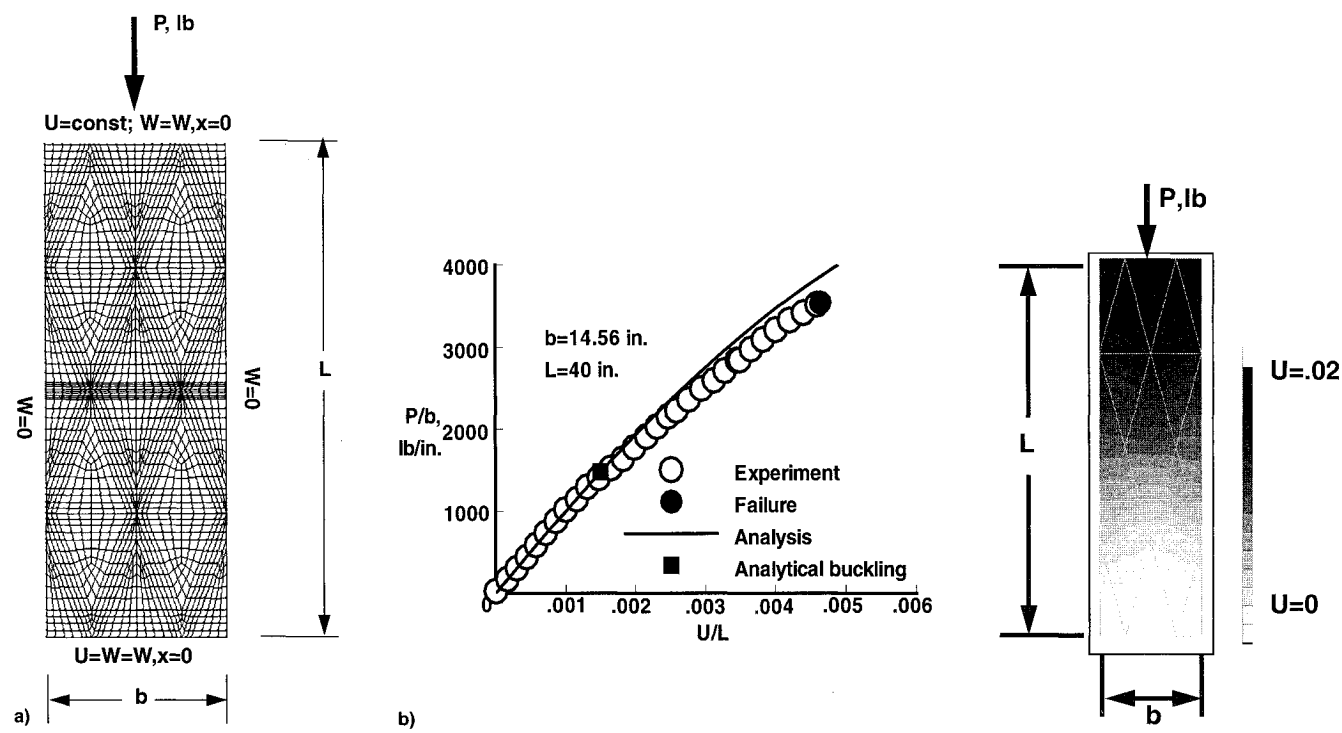

Fig. 11 Comparison of experimental and analytical results for panel specimen: a) finite element model and b) end-shortening results.

half-model of specimen E4 and is expected to exhibit a response similar to specimen E4. Specimen E4 has slightly larger average in-plane stiffness, as suggested by the slope of the curve, since the stiffener crossover region contributes to the stiffness. The failure loads for these two specimens are only slightly different. The specimen E1 with a single stiffener exhibited behavior typical of a 0-deg laminate and failed at an average strain of 0.01275 in./in. Specimen E2, which is made of a straight stiffener and a crossover region, has the greatest axial stiffness and the lowest failure load of the element specimens evaluated. The failure is because of skin stiffener separation and occurs at much lower load than the other types of element specimens. Typical out-of-plane displacement profiles for specimens E3 and E4 before failure obtained from shadow moiré interferometry and the corresponding failure modes are presented in Fig. 9. Skin buckling can be seen very clearly in all of the cases and results in large interlaminar stresses at the skin-stiffener interface region. These interlaminar stresses seem to eventually initiate failure as the panel is loaded into the postbuckling region.

Damaged Compression Panels

Experimental results for a geodesic compression panel subjected to low-speed impact damage are presented in Fig. 10. A 14.56-in.-wide panel was subjected to low-speed impact damage normal to the skin surface at two locations near the skin-stiffener interface prior to testing. Aluminum spheres 0.5 in. in diameter were used as the impact projectile in this investigation. The panel was impacted at a point midway between intersecting stiffeners with a speed V_1 of 345 ft/s and at the intersection of two stiffeners with a speed V_2 of 350 ft/s. These impact locations are shown in Fig. 10. There was observable damage in the panel corresponding to the impact energy levels used. No additional nondestructive evaluations were performed to quantify the impact damage. The plot on the left of the figure shows normalized end-shortening deflection as a function of normalized applied load. Failure of the undamaged and impact-damaged panels is represented by the filled circles. The theoretical buckling load of an undamaged panel is represented by the open circle. The results show that the impact-damaged panel failed at a normalized load of approximately 2900 lb/in., which is slightly lower than the failure load of the panel tested without low-speed impact damage. The photograph on the right of the figure shows the failed impact-damaged panel. The photograph shows that the panel failed in a mode similar to that for the undamaged panel that was shown in Fig. 7. The results presented in Fig. 10 suggest that the presence of low-speed impact damage did not significantly influence the stiffness or strength of this geodesically stiffened compression panel.

Table 1 Typical graphite-epoxy material properties

Longitudinal Young's modulus, 17.0 Msi
Tranverse Young's modulus, 1.7 Msi
Shear modulus, 0.65 Msi
Major Poisson's ratio 0.30
Tape nominal ply thickness, 0.0107 in.
Fabric nominal ply thickness, 0.0217 in.

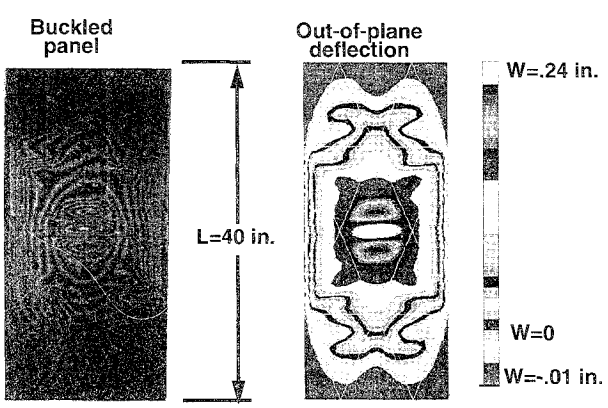

Fig. 12 Comparison of experimental and analytical out-of-plane displacement results for a 14.56-in.-wide panel.

Analytical Results

Panel Global Response

A finite element model for the panel specimen is shown in Fig. 11a. The material properties used in the analysis are shown in Table 1. The skin, stiffeners, and frame clips were modeled with quadrilateral plate elements that allow transverse shear deformations. The finite element model of the 14.56-in.-wide panel had 2900 quadrilateral plate elements with approximately 18,000 degrees of freedom. Boundary conditions shown in Fig. 11a were assumed along the edges of the panel. The loading condition used for the analyses was a uniform end-shortening applied to one end of the specimen. The U displacement degree of freedom was constrained at the opposite edge. The out-of-plane deflections W were constrained along all the edges of the panel. A comparison between test results and analytical results obtained using the structural analysis of general shells (STAGS) computer code (Ref. 9) is presented in Fig. 11b. A finite element analysis was used to perform linear and geometrically nonlinear analyses of panel global response. Normalized end-shortening results as a function of normalized load are shown on the left of the figure. The open circles represent experimental results and the line represents analytical results. The filled circle denotes failure of the panel and the filled square denotes the analytical buckling load obtained from linear buckling calculations using the STAGS finite element code. End-shortening displacement contours calculated from a geometrically nonlinear finite element analysis are shown on the right of the figure. The contour results indicate that applied end-shortening was uniform across

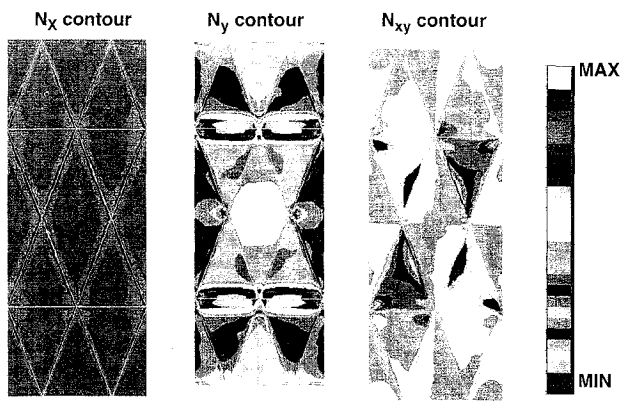

Fig. 13 Typical stress resultant contour results from panel specimen nonlinear analysis.

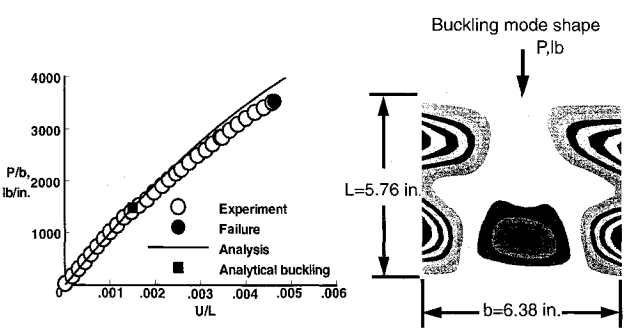

Fig. 14 Comparison of experimental and analytical results for element specimen E3.

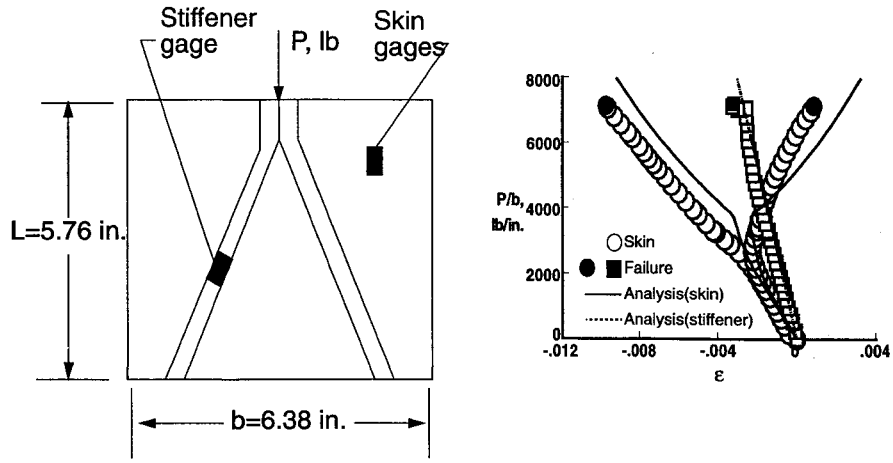

Fig. 15 Comparison of typical experimental and analytical strain results for element specimen E3.

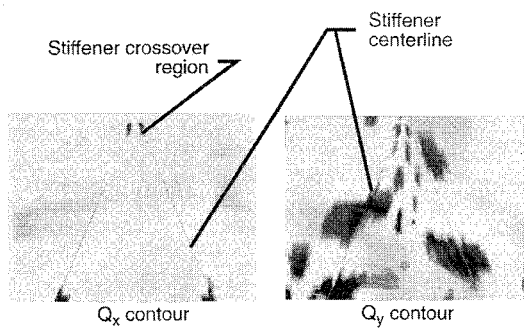

Fig. 16 Typical transverse shear stress resultants contours for element specimen E3.

the width at the loaded edges of the panel. However, the end-shortening displacement contours were not uniform across the width of the panel away from the loaded edges. The results suggest that the end-shortening displacement contours were influenced by the stiffeners and stiffener intersection points. The results presented in Fig. 11 indicate that the analysis accurately predicts the panel end-shortening response up to buckling. The difference between analytical and experimental post-buckling responses of the panel may be attributed to local failures at buckling that result in reduced panel stiffness.

Finite element results for the out-of-plane deflections W at approximately 1.5 times the buckling load and a photograph of the corresponding moiré-fringe pattern are presented in Fig. 12. A photograph of the moiré-fringe pattern for the skin side of a 14.56-in.-wide panel is shown on the left of the figure. This photograph shows that the rhombic skin panel region buckled into three half-waves at the center of the panel. The analytical out-of-plane deflection contours presented on the right of the figure compare well with experimental results. The out-of-plane deflection results presented in the figure also indicate that the center region of the entire panel deformed out-of-plane during loading. Also, the buckling mode of the rhombic skin region has three half-waves with a noticeable skew. The shear stress in the rhombus-shaped skin region because of compression loading of the panel introduces this skewing of the buckling pattern.

Typical stress resultant contours for a 14.56-in.-wide specimen calculated from a geometrically nonlinear finite element analysis at approximately 1.5 times buckling load are presented in Fig. 13. Contour plots of the in-plane normal stress resultants N_x, in a direction parallel to the longitudinal axis of the panel and along the axis of the stiffeners and frame clips, are shown on the left of the figure. The contour results indicate that most of the compression load is carried by the stiffeners of the geodesic compression panel. Contour plots of the in-plane normal stress resultants N_y (in a direction normal to the longitudinal axis of the panel), are shown on the middle of the figure. These results indicate that the stress resultants normal to the longitudinal axis of the panel are maximum near the location of frame clips where the 0-material buffer strips were embedded into the skin laminate. The high N_y stress resultants at the location of the frame clips are because of the buffer strips resisting the lateral movement of the stiffeners at the stiffener intersection. The in-plane shear stress resultant N_{xy} distribution is presented on the right of Fig. 13. These results indicate that the rhombic skin region in the middle of the panel is subjected to shear loads in addition to the axial compression loads, and explains the skewing of the buckling mode shape for this skin region.

Element Specimen Failure

From the element specimen test results presented in Figs. 8 and 9, the response mechanisms for specimens E3 and E4 are more representative of the large panel response rather than specimens E1 and E2. For this reason, understanding failure mechanisms associated with one of these specimens is expected to provide insight into the failure of the large panel. A detailed STAGS model for specimen E3 has been generated to perform nonlinear analyses to help understand the failure mechanisms for this specimen. The experimental end-shortening results for this specimen are compared with the analysis results for element specimen E3 in Fig. 14. The nonlinearity in global response is predicted very accurately by the analysis. The analytical buckling mode shape for the element specimen is shown in the inset, which matches the experimentally observed out-of-plane displacement contour for the element specimen shown in Fig. 9. The analytical buckling mode shape for the element specimen also corresponds to that for the rhombic skin region at the center of the large panel shown in Fig. 12.

Typical experimental in-plane strain results at skin and stiffener locations for specimen E3 are compared with the corresponding analysis results in Fig. 15. Buckling of the skin outside of the stiffeners is predicted to occur for a load of 3800 lb/in., which is more than the experimental buckling load. The analysis results for strain exhibit the same trend as the experimental results both at the skin and stiffener locations shown in Fig. 15. The discrepancy in skin strain results may be because of local failures in the skin prior to and at buckling as indicated by jumps in end-shortening data in Fig. 14. The distribution of resultant shear stresses for the buckled specimen at a load value that is four times the skin buckling load are presented in Fig. 16. These shear stress concentrations at a corner point of the stiffener crossover region indicate that failure of the skin-stiffener flange interface may have initiated at this location with subsequent skin failure.

Concluding Remarks

An experimental and analytical investigation has been conducted to study the structural response of geodesically stiffened graphite–epoxy compression panels. Results are presented for panels that were tested with and without low-speed impact damage. Analytical results from linear and nonlinear finite element analyses are also presented and compared with experimental results. The experimental results suggest that local buckling of the skin preceded panel failure, which occurs at approximately four times the skin buckling load. Low-speed impact damage at energy levels used in this study did not significantly reduce the load carrying capability of the geodesically stiffened compression panels tested. Analytical results suggest that the stiffeners carried most of the load compared to the skin. In-plane stress resultants normal to the longitudinal direction of the panel were maximum near buffer strips embedded in the skin of the panel and resist in-plane lateral deformation of the stiffeners at stiffener intersections. This structural concept demonstrated the ability of the buffer strips to function as embedded stiffeners in the lateral direction while used as fail-safe straps. The correlation between analytical and experimental results confirms the adequacy of the finite element representations used in the study. Skin-stiffener separation and skin failure close to the intersection of stiffeners along the horizontal centerline caused failure of the geodesically stiffened panels. Nonlinear analysis results for an element specimen suggest that a shear stress concentration exists at the corner point of the stiffener crossover, which may have initiated failure in the panel specimen.

References

[1]Rehfield, L. W., Deo, R. B., and Renieri, G., "Continuous Filament Advanced Composite Isogrid: A Promising Structural Concept," *Fibrous Composites in Structural Design*, Plenum, New York, 1980, pp. 215–239.

[2]Rehfield, L. W., Reddy, A. D., Yehezkely, O., and Armanios, E. A., "Buckling of Continuous Filament Composite Isogrid Panels: Theory and Experiment," *Progress in Science and Engineering of Composites*, ICCM-IV, Tokyo, 1982, pp. 545–553.

[3]Rehfield, L. W., and Reddy, A. D., "Damage Tolerance Studies on Continuous Filament Graphite/Epoxy Isogrod Structures," *Composite Materials, Mechanics, Mechanical Properties and Fabrication, Japan Society for Composite Materials*, edited by K. Kawata and T. Akasaka, Toyko, 1981, pp. 471–477.

[4]Reddy, A. D., Haag, R., Widmann, C. G., and Rehfield, L. W., "Compressive Buckling Behavior of Graphite/Epoxy Isogrid Wide Columns with Progressive Damage," *Compression Testing of Homogeneous Materials and Composites*, edited by R. Chair and R. Papirno, American Society for Testing and Materials STP 808, 1983, pp. 187–199.

[5]Reddy, A. D., Valisetty, R. R., and Rehfield, L. W., "Continuous Filament Wound Grid Stiffened Composite Structures for Aircraft Fuselages," *Journal of Aircraft*, Vol. 26, No. 2, 1985, pp. 249–255.

[6]Anderson, R. G., "Manufacturing of the Army/Bell Advanced Composite Helicopter Airframe," *Proceedings of the American Helicopter Society, Composite Structures Specialist's Meeting* (Philadelphia, PA), American Helicopter Society, Washington, DC, 1983.

[7]Phillips, J. L., "Structural Analysis and Optimum Design of Geodesically Stiffened Composite Panels," M.S. Thesis, Virginia Polytechnic Inst. and State Univ., Blacksburg, VA, Feb. 1990.

[8]Wiggenraad, J. F. M., and Bauld, N. R., Jr., "Global/Local Interlaminar Stress Analysis of a Grid-Stiffened Composite Panel," *Journal of Reinforced Plastics and Composites*, Vol. 12, Feb. 1993, pp. 237–253.

[9]Brogan, F. A., Rankin, C. C., and Cabiness, H. D., "STAGS User Manual," Lockheed Palo Alto Research Lab., Rept. LMSC P032594, 1994.